Zernike phase contrast in high-energy x-ray transmission microscopy based on refractive optics

KEN VIDAR FALCH[A], MIKHAIL LYUBOMIRSKIJ[B], DANIELE CASARI[A], ANATOLY SNIGIREV[C], IRINA SNIGIREVA[B], CARSTEN DETLEFS[B], MARCO DI MICHIEL[B], IVAN LYATUN[C], AND RAGNVALD H. MATHIESEN[A,*]

[a]*Norwegian University of Science and Technology, Department of physics, Høgskoleringen 1, 7491 Trondheim, Norway*
[b]*European Synchrotron Radiation Facility, 71 Avenue des Martyrs, 38000 Grenoble, France*
[c]*Immanuel Kant Baltic Federal University, 238300 Kaliningrad, Russia*

A B S T R A C T

The current work represents the first implementation of Zernike phase contrast for compound refractive lens based x-ray microscopy, and also the first successful Zernike phase contrast experiment at photon energies above 12 keV. Phase contrast was achieved by fitting a compound refractive lens with a circular phase plate. The resolution is demonstrated to be sub-micron, and can be improved using already existing technology. The possibility of combining the technique with polychromatic radiation is considered, and a preliminary test experiment was performed with positive results.

1. Introduction

X-ray microscopy is a powerful technique that allows non-destructive study of a wide range of natural and man-made objects with sub-micron spatial resolution. In the most straight forward implementation, the main contrast mechanism is absorption. Consequently, it can be difficult or impossible to obtain high quality images in cases where the absorption contrast is weak. Zernike phase contrast (ZPC) is a microscopy technique that produces phase contrast by converting phase modulations into detectable amplitude modulations. It has been used frequently with visible light optics since its introduction in 1942 [1]. With X-rays, ZPC microscopy was first demonstrated in 1994 at photon energies ~0.5 keV, employing Fresnel Zone Plates (FZPs) [2]. Similar FZP based setups have since been used to obtain ZPC microscopy images with resolution in the 40-100 nm range at energies 4-8 keV [3-5]. Scanning ZPC has also been demonstrated with promising results, allowing for spectroscopic mapping [6]. Furthermore, efforts have been made to extract quantitative phase information by alternating between negative and positive ZPC. Numerical results employing this technique were published quite recently [7].

The potential of ZPC makes it a promising direction for development of microscopy based on Compound Refractive Lenses (CRLs). While existing CRLs cannot match FZPs when it comes to resolution, they can be used at photon energies well above those currently feasible with FZP optics. Use of high energy x-rays is advantageous for microscopy of e.g. inorganic samples of appreciable thickness in order to have a usable amount of transmission through the sample, and often also to reduce sample alteration or damage associated with ionization. Microscopy based on CRLs has been demonstrated at energies up to 50 keV [8], and could quite readily be extended to operate at even higher energies. ZPC at 25 keV was reported in 2003 [9], based on refractive capillary lenses, and represents until now the only X-ray ZPC study reported based on refractive optics. Since then, however, refractive x-ray optics has vastly improved. This study presented the first results of combining ZPC with modern CRLs, and may represent an important and necessary step in the development of refractive x-ray optics, and is of particular relevance for x-ray microscopy at high photon energies.

2. Experimental setup

An experiment was performed at the micro optics test bench at beamline ID06 at the European Synchrotron Radiation Facility. The experimental setup is illustrated in Figure 1. The condenser images the source onto the phase plate, which is situated inside the objective. With absorbing CRLs, placing the source image inside the objective has the positive effects of optimizing transmission [10] and reducing field curvature stemming from spherical aberrations in the objective. Additionally, when polychromatic illumination is used, this configuration eliminates lateral chromatic aberrations [11]. For standard microscopy, a potential drawback might be that the illumination may not fill the aperture of the objective unless a suitable beam diffuser is employed. With ZPC, however, the allowable angular distributions of the illumination are always dictated by the shape and dimensions of the phase element. The objective CRL is positioned so that an image of the sample is formed on the detector. The microscope was operated on an undulator source with 17 keV radiation selected by liquid nitrogen cooled Si(111) double-crystal fixed exit monochromator, and with the sample and detector placed 800 mm upstream and 4200 mm downstream of the objective, respectively. The detector was a pco.2000 CCD camera equipped with 10x visible light optics and a Eu-doped GdGa-garnet crystal scintillator. Both the condenser and objective were made by assemblies of double concave 50 µm apex radius Be-lenslets. The condenser

consisted of 16 lenslets with 2 mm spacing, resulting in a total thickness of 32 mm, while the objective contained 32 lenslets with thickness 1.6 mm. In the objective, a 5 mm spacer was inserted between the 16th and the 17th lenslet with its interior open for the beam to pass through and so that a phase plate could be suspended into the opening from above. Ideally, the phase element would be attached and aligned to the spacer. The total length of the objective, including the spacer, was 56 mm.

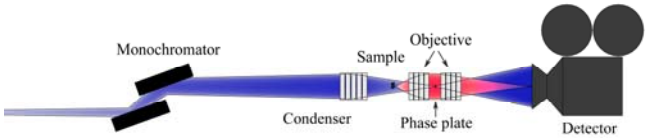

Fig 1: Schematic illustration of the experimental setup.

The phase plate was a 1.7 µm thick 30 µm diameter platinum disc mounted on a silicon nitride membrane, which at 17 keV induces a phase shift of 0.56π. The numerical aperture of the objective was estimated to N.A.=2.8×10^{-4} considering the marginal rays from the sample. The geometrical aperture was significantly smaller than the Gaussian effective aperture defined by absorption in the lens material. The root-mean-square (RMS) source size at ID06 is 415 µm and 8.6 µm in the horizontal and vertical directions, respectively. The distance between the condenser and the source was 53 m while the distance between the condenser and the objective was 1.3 m. A rough estimate of the spot size on phase plate, R_{bg}, can be obtained by multiplying the horizontal source size by the demagnification of the source image, which yields $R_{bg}\approx10$ µm.

Another test experiment was performed at beamline ID31 at the European Synchrotron Radiation Facility. The setup was similar to the previous one with the sample and detector placed 425 mm and 5000 mm upstream and downstream of the objective, respectively. The objective and condenser contained 87 and 32 Be-lenslets, respectively, each with 50 µm apex radius. In this experiment the incident beam photon energy was 22.5 keV selected by two multilayer mirrors, which results in a bandwidth of 0.3 % rather than the typical 0.01% bandwidth from a Si(111) double-crystal monochromator. A collector lens consisting of 5 Be-Lenslets with 200 µm apex radii was situated about 31 m from the source, which was 117 m upstream of the sample position. The main objective for this study was to verify that ZPC imaging could be carried out with satisfactory results also with non-monochromatic radiation.

If ZPC is to be employed for ultra-fast imaging, like e.g. time-resolved in situ tomography, it would be an advantage if it could be used in combination with broadband radiation. However, the significantly increased photon flux could potentially cause substantial heating or even melting of the phase element, in particular taking into account that the phase element would be placed in the focal spot of the condenser. Therefore, rather than using a phase plate, a hole was made in the center of one of the lenslets. This lenslet will be referred to as a Zernike lenslet. The nominal web thickness of the lenslet was 30 µm, which gives the background wave a phase shift of φ=-π/2-0.23π. The diameter of the hole was 20 µm. After the microscope was aligned with a standard CRL objective, the central lenslet was replaced by the Zernike lenslet.

3. Theory

The ray transfer matrix for a complete microscope, from sample to detector, is

$$M_p = \cos(\omega L)\begin{bmatrix} 1-\frac{q}{F} & p+q+\frac{pq}{F}+\frac{1}{F\omega^2} \\ -\frac{1}{F} & 1-\frac{p}{F} \end{bmatrix} \quad (1)$$

where p and q are the distances from the sample to the objective entrance and from the objective exit to the detector, as illustrated in Figure 2, and $\omega = (fT)^{-\frac{1}{2}}$, where f and T are the focal length of a single lenslet and the spacing between lenslets, respectively. F is the focal length measured from the exit of the lens, given by

$$F = \frac{1}{\omega\tan(\omega L)} \quad (2)$$

with L as the length of the CRL. The imaging condition is met when the upper right element of M_p vanishes, i.e. when

$$\frac{1}{F}-\frac{1}{p}-\frac{1}{q}-\frac{1}{pqF\omega^2}=0. \quad (3)$$

The image formed by a microscope can be considered as a sum of the scattered wave field and the non-scattered background wave field. In absorption contrast, the scattered wave is approximately π/2 out of phase with respect to the background wave, assuming small phase variations in the sample. The core principle of ZPC is to phase shift the background wave by ±π/2 so that it may interfere with the scattered wave. This way, phase variations in the scattered wave can produce intensity variations in the final image. The phase shift can be achieved by placing a phase shifting element, such as a plate- or a ring structure, in the Fourier plane where the scattered wave appears as the Fourier transform of the sample and the background wave comes to a focus. In the Fourier plane the scattered wave and background wave are separated, allowing the phase element to discriminate between the two. In the conceptually simplest form of ZPC imaging, the sample is illuminated by a coherent plane wave. In this case, the ideal phase element would be a disc placed in the back focal plane of the objective. By adding a condenser lens upstream of the sample, the focus of the background wave, and thus the ideal place for the phase element, is moved along the optical axis.

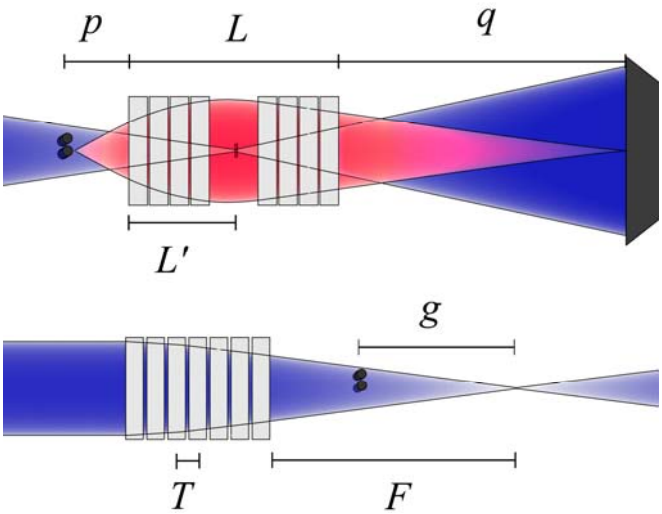

Fig 2: Illustration of the meaning of CRL parameters.

Fringes related to absorption in the objective are common artefacts in CRL-based microscopy [12]. The severity of the effect increases with decreasing effective objective aperture and with the distance from the

sample feature to the optical axis. At high energies, where the effective aperture for a given resolution is likely to be smaller, the effect is expected to become more pronounced. The fringes occur because the Fourier plane is not located in the effective aperture stop plane. Often in CRL microscopy, the objective lens itself will act as the aperture stop. The fringes can be removed by moving the Fourier plane to the effective aperture stop. This is equivalent to aligning the background wave with the principle rays, which can be done with the help of a condenser lens. The principle ray through a system of CRLs without diaphragms is the ray that maximizes the transmission from the sample plane to the image plane. In most cases, simply focusing the background wave somewhere inside the objective is good enough.

In cases with long objectives, the principle rays can be determined by finding the initial ray angle that maximizes the transmission. The transmission of a ray through a CRL is a Gaussian function of position, r, and angle, w, of the ray at the objective entrance. [13]. It may therefore be expressed as

$$t(\mathbf{x}) = e^{-\mu T_w N} e^{-\frac{1}{2}\mathbf{x}^T \Sigma^{-1} \mathbf{x}} , \tag{4}$$

Where T_w is the web thickness, μ is the mass attenuation coefficient of the CRL material, and $\mathbf{X}$ is a ray vector with r and w as its first and second element, respectively. and Σ^{-1} is a 2×2 matrix whose elements depend on the CRL parameters. Specifically

$$\Sigma^{-1} = \gamma k \begin{bmatrix} \omega(\omega L + \frac{1}{2}\sin(2\omega L)) & \sin^2(\omega L) \\ \sin^2(\omega L) & \dfrac{\omega L - \frac{1}{2}\sin(2\omega L)}{\omega} \end{bmatrix} . \tag{5}$$

From this, the transmission of a ray from the sample plane can then be found by mapping them to the objective entrance. The mapping is done by multiplying $\mathbf{x}$ with the free propagation matrix

$$\mathbf{R}(p) = \begin{bmatrix} 1 & p \\ 0 & 1 \end{bmatrix} . \tag{6}$$

Substituting $\mathbf{x}_i = \mathbf{R}(p)\mathbf{x}$ into (4) yields

$$t_i(\mathbf{x}_i) = e^{-\mu T_w N} e^{-\frac{1}{2}\mathbf{x}_i \Sigma_i^{-1} \mathbf{x}_i} , \tag{7}$$

where

$$\Sigma_i^{-1} = \mathbf{R}^T(p) \Sigma^{-1} \mathbf{R}(p) . \tag{8}$$

For a given r, the angle w_p of the principle ray must be the w_0 that maximizes t_0. This angle can be expressed in terms of the elements of Σ_i^{-1} as

$$w_p = -\frac{\Sigma_{i,(1,2)}^{-1}}{\Sigma_{i,(2,2)}^{-1}} r_0 . \tag{9}$$

Let g be the distance from the sample to where the illumination would come to a focus if objective lens was not present. By choosing

$$g = -\frac{r_0}{w_p} = \frac{\Sigma_{0,(2,2)}^{-1}}{\Sigma_{0,(1,2)}^{-1}} , \tag{10}$$

the illumination is aligned with the principle rays. By ray tracing, the distance L' from the objective entrance to the Fourier plane can be related to g by

$$g = p + \tan(\omega L')/\omega , \tag{11}$$

which may be satisfactory approximated by $g \approx p + L'$ for short or weakly refracting CRLs.

In order to determine the appropriate size of the phase plate it is necessary to relate the spatial displacement in the Fourier plane to reciprocal components of the sample transmission function. For this, it is convenient to calculate the ray transfer matrix M' that maps rays from the sample plane to the Fourier plane.

$$\begin{aligned} M' &= \begin{bmatrix} \cos(\omega L') & \dfrac{\sin(\omega L')}{\omega} \\ -\omega \sin(\omega L') & \cos(\omega L') \end{bmatrix} \begin{bmatrix} 1 & p \\ 0 & 1 \end{bmatrix} \begin{bmatrix} 1 & 0 \\ -\frac{1}{g} & 1 \end{bmatrix} \\ &= \begin{bmatrix} 0 & p\cos(\omega L') + \dfrac{\sin(\omega L')}{\omega} \\ \dfrac{\omega}{\sin(\omega L')} - \dfrac{1}{p\cos(\omega L')} & \cos(\omega L') - \omega p \sin(\omega L') \end{bmatrix} \end{aligned} \tag{12}$$

A displacement $\mathbf{r}_{FT}$ in the Fourier plane can then be related to the reciprocal coordinate $\mathbf{q}$ by

$$\mathbf{q} = \frac{k}{B'} \mathbf{r}_{FT} \tag{13}$$

where $k = 2\pi/\lambda$ is the wavenumber, λ the wavelength, and

$$B' = p\cos(\omega L') + \sin(\omega L')/\omega \tag{14}$$

is the upper right element of M'. The mapping of the phase plate radius R_p to the radius R_q of the affected region in reciprocal space is

$$R_q = \frac{k}{B'} R_p , \tag{15}$$

The lower limit of R_p is determined by the numerical aperture of the condensing optics, the longitudinal alignment precision, and the illumination coherence length. At synchrotrons, assuming no diffusing element is being used, the coherence length is mainly related to the angular source size, which gives rise to a smearing of the intensity profile in the Fourier plane. As a result, the phase plate cannot effectively discriminate between the background and scattered wave when scattering angles become comparable to the angular source size. This implies that at high energies, the source size may have to be taken into consideration.

The minimum size of R_p is related to the size of the background wave in the Fourier plane. It is assumed that the beam is condensed by a CRL with Gaussian aperture, and that the root-mean-square (RMS) source size is σ_s. Hence, the RMS size of the background wave can be expressed

$$\sigma_{bg}^2 = \sigma_s^2 m_s^2 + \Delta g^2 \sigma_{\mathrm{N.A.}'}^2 + \frac{1}{4k^2 \sigma_{\mathrm{N.A.}'}^2} , \tag{16}$$

where m_s is the source demagnification, Δg is the misalignment between the Fourier plane and phase element, and $\sigma_{\mathrm{N.A}}$ is the RMS of the numerical aperture of condenser combined with any objective lenslets upstream of the phase plate. The third term on the right hand side of (16), relates to the diffraction limit, and is practically negligible. Although this expression is specific to phase discs, the same qualitative results are expected for phase elements of other shapes. As a Gaussian function is non-zero in the whole domain, the phase plate is defined to be covering the beam when

$$R_{\mathrm{p}} = C\sigma_{\mathrm{bg}} \tag{17}$$

is satisfied, corresponding to a coverage of the beam intensity profile at a C·σ level when the beam is centered on the phase plate.

The upper limit of R_p is not as sharply defined as the lower limit. The larger the object, the smaller the phase plate needs to be. Although the shape of the object matters, a reasonable rule of thumb is to keep $R_{\rho}\rho \approx 1$ [14], where ρ is the radius of the largest object required to be fringe free. In real space, this translates to a maximum plate radius of

$$R_{p,\max} \approx \frac{B'}{k\rho} \tag{18}$$

The pending question is how $R_{p,\max}$ develops with increase in the photon energy. For a given energy, B' depends on the parameters of the objective as well as the geometry of the setup. A complete mapping of all possibilities is not reasonable as constraints set by the ability to produce lenslets with certain thicknesses and apex radii in the end will be the real limiting factors. Figure 3 was produced assuming Be-lenslets with T=1.6 mm and R_a=50 µm, corresponding to the most readily available Be-lenslets at present. The figure shows B'/k as a function of the diffraction limit r_d for different energies. The calculation was done in the limit of infinite magnification, which maximizes the diffraction limit and is equivalent to $p=F$.

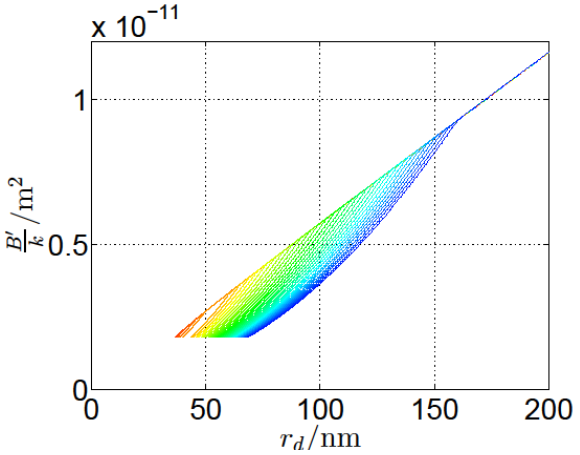

Fig 3: B'/k as a function of r_d. The energy range is 15-100 keV. There is a 2.5 keV gap between each line. The red and blue lines at the extremes represent 15 keV and 100 keV, respectively. The calculation was done by estimating B'/k and r_d in the limit of infinite magnification. It is assumed that the illumination is focused so that the non-scattered wave follows the principle rays, in accordance with to (10). The common asymptote is related to the geometrical aperture, and can be calculated as $B'/k \approx Ar_d/(0.61\cdot 4\pi)$, where A is the geometrical aperture.

For it to be possible to satisfy both the upper and lower constraint one must have $C\sigma_{\mathrm{bg}} < 2\pi B'/k\rho$. The maximum photon energy where this occurs iss

$$E_{\max} = 2\pi\hbar c\frac{B'}{C\sigma_{\mathrm{bg}}\rho} \tag{19}$$

Where $\hbar$ is the reduced Planck's constant and c is the speed of light in vacuum. It should be kept in mind that in practice B' as well as m_s will be energy dependent. .

It was recently demonstrated that lateral chromatic aberration is corrected by using the illumination scheme considered here [11]. The possibility of using ZPC with non-monochromatic illumination with band width is in the range $\Delta E/E \sim 10^{-2}$, commonly referred to in the synchrotron radiation community as a pink beam, will now be considered. A numerical experiment considering a CRL microscope with unit magnification and parallel pink beam illumination has already given promising results [15]. The two main concerns when it comes to ZPC with a pink beam is the energy dependence of both the phase shift induced by the phase plate, and the spread of Fourier planes due to the chromaticity of the condenser.

The phase shift, φ, induced by the phase plate is proportional to δ, which in turn is proportional to E^{-2}. The amplitude of the intensity modulation due to interference between scattered and background wave is proportional to the deviation $\tau = \sin(\varphi)$. Let the phase shift induced at the central energy in the ΔE energy range be denoted by φ_0. The spread in phase shifts is

$$\Delta\varphi \approx 2\varphi_0\frac{\Delta E}{E} \tag{20}$$

Using $\Delta E/E = 10^{-2}$, assuming $\varphi_0 = \pi/2$, and evaluating τ at the marginal energies of the spectrum yields

$$\tau = \cos\left(\tfrac{1}{2}\Delta\varphi\right) \approx 1 - 10^{-4}\,\tfrac{\pi^2}{4}. \tag{21}$$

This is close to one, and still would be even if the bandwidth was increased by an order of magnitude. Thus one may conclude that phase shift spread is not likely to be a problem with a pink beam illumination.

The location of the Fourier plane will vary with energy. If Δg_{ch} is the Fourier plane misalignment of the lowest and highest contributing frequency in the spectrum, and if it is assumed that Δg_{ch} is significantly larger than the alignment accuracy,

$$\sigma_{\mathrm{bg}}^2 = \sigma_s^2 m_s^{\,2} + \Delta g_{\mathrm{ch}}^{\,2}\sigma_{\mathrm{N.A.'}}^2 + \frac{1}{4k^2\sigma_{\mathrm{N.A.'}}^2}. \tag{22}$$

4. Results and discussion

For each recorded image, a flat field image and a dark frame was also recorded. The final results presented are the flat field corrected images, where both the raw images and flat fields were dark frame subtracted. The images in Figure 4-7 were recorded with the monochromatic setup, while the image in Figure 9 was recorded with the pink beam setup and a Zernike lenslet.

Figure 4-7 shows ZPC and reference images of 2 µm diameter polystyrene colloidal spheres, a 20 µm thick beryllium electron microscopy grid, the microstructure of an Al-Si alloy, and a boron fiber with an interior tungsten core, respectively. Exposure times of 1 s and 0.6 s for the ZPC and reference images, respectively, were chosen to stay well below the saturation limit of the CCD. In all cases the reference image was recorded with the exact same setup, with the exception that the phase plate was removed from the CRL (insertable/removable by a stepper motor). The sample for the pink beam image seen in Figure 8 was a 2000 mesh Cu microscopy grid with 8 µm diameter holes.

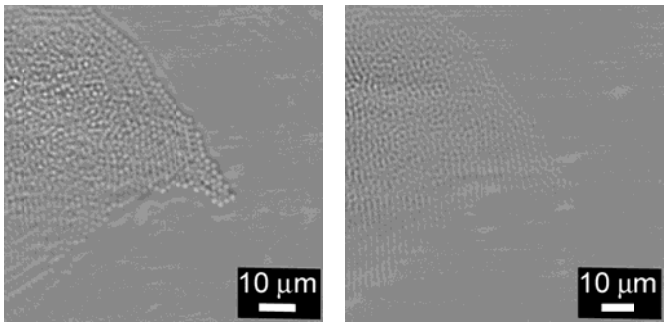

(a) (b)

Fig 4: ZPC image (a) and reference image (b) of 2 µm polystyrene colloidal particles.

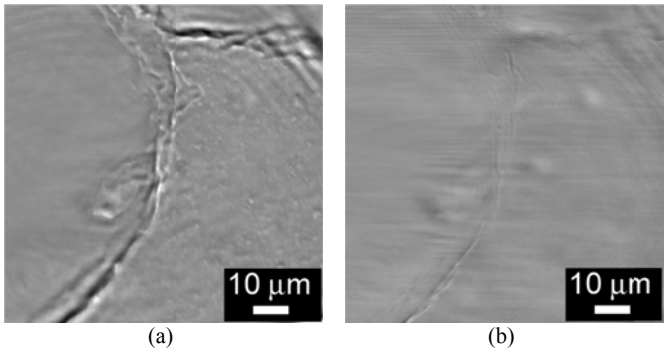

(a) (b)

Fig 5: Zernike phase contrast (a) and reference (b) images of a beryllium microscopy grid.

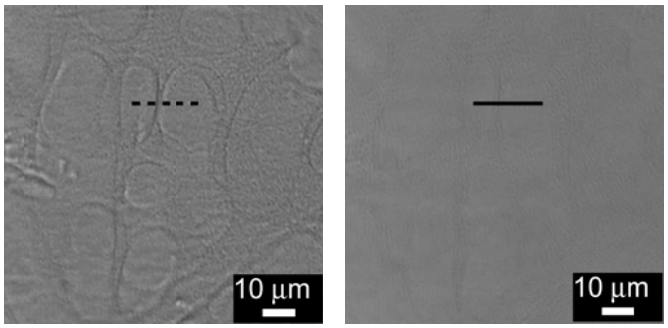

(a) (b)

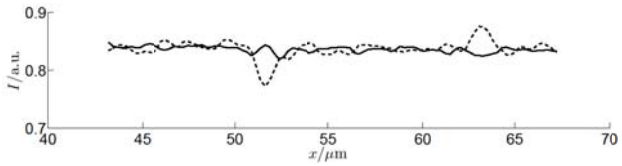

(c)

Fig 6: Zernike phase contrast (a) and non-ZPC reference (b) images of a 200 µm thick Al-Si alloy sample. (c) Intensity profile sampled from the black lines using bilinear interpolation.

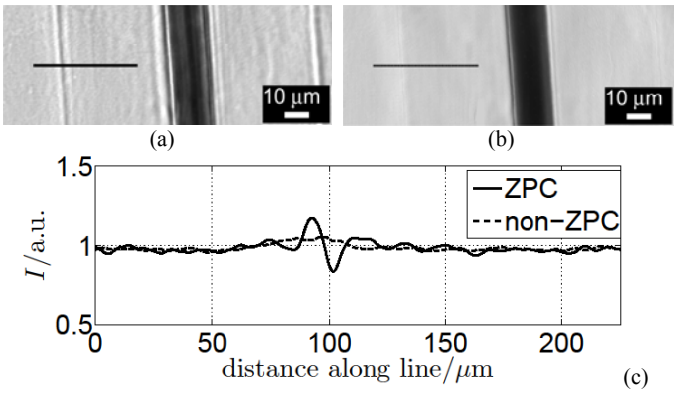

(a) (b) (c)

Fig 7 : Zernike phase contrast (a) and absorption contrast (b) images of a boron fiber with a tungsten core. (c) Intensity profile sampled from the black lines using bilinear interpolation.

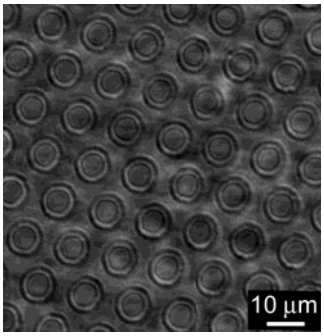

Fig 8: Zernike phase contrast Image of a 2000 mesh Cu microscopy grid with 8 µm diameter holes, recorded with 22.5 keV radiation with 0.3% bandwidth.

In Figure 4a the polystyrene spheres appears with inverted contrast compared to the non ZPC reference image in Figure 4b. The attenuation through 2 µm polystyrene is approximately 0.01% at 17 keV, but the colloidal particles are still visible without any phase shifting element due to scattering and propagation-based phase contrast. Taking the radius of the spheres as ρ, $R_{\phi}\rho$=1.7. Ringing artefacts are present, but faint. Although it is difficult to pin down beyond doubt the contrast mechanism at work in in Figure 4a, contrast inversion is consistent with ZPC. The essence of ZPC is the induction of a relative phase shift between the background and signal, which may result in contrast inversion. In this experiment, the non-scattered background wave was phase shifted in the same direction as the scattered wave, resulting in positive interference, and thus positive contrast from the spheres.

The advantage of ZPC in hard x-ray microscopy is perhaps most evident in Figure 5. Although some scattering contrast and propagation-based phase contrast appear in the reference image Figure 5b, the ZPC image reveals details that are barely visible in the reference. Likewise, in Fig 6, the boundaries between primary-phase Al-dendrites and Sr-modified fibrous Al-Si eutectic microstructures [16] are readily visible in the ZPC image. In the reference image, faint contrast features, barely detectable above the noise level, can be found between the coarse primary dendrites and the surrounding eutectic, whereas the finer internal eutectic microsctructure features remain unresolved. The absorption contrast between Al and Si at 17 keV is negligible. As the eutectic regions consists of 3D layers of micron-sized overlapping features, it is not clear whether the ZPC image represents an accurate 2D projection of the sample, which is a necessity for tomographic applications. Further experiments are necessary to determine if the setup can be used to obtain tomograms of the eutectic microstructure.

The spatial coherence of the illumination in combination with imperfections in beamline components used in the experiments typically gives a rise to speckles and features in the illumination intensity. The uneven illumination is particularly evident in Figure and 5 where large horizontal fringes are visible, presumably stemming from defects in the condenser. These features can be mitigated by decohering the illumination, simply by inserting a diffuser somewhere upstream of the sample. A suitable diffuser could be a rotating disc made from a low-absorbing semi-amorphous or ultra-fine grained material. Unfortunately, decohering comes at the cost of smearing the focal spot in the Fourier plane. ZPC requires the diffuser to be gentle enough so that the background and the scattered wave still can be discriminated.

Figure 7 shows images of a weakly absorbing boron fiber with a heavily absorbing tungsten core. The border between the boron and the surrounding air is dramatically more visible with ZPC, however, halo artefacts are quite visible. $R_q\rho$ was 88.3 with ρ as the radius of the boron fibre. Apart from using smaller phase plates, a number of techniques exist for apodization [17-19], but adaptation of these techniques to CRL microscopy is not necessarily straight forward without sacrificing considerable amounts of flux. Smoothing the edge of the phase plate can also have a positive effect [14]. An investigation into which apodization methods might be suitable for hard x-ray CRL microscopy could be a topic for future investigations.

Figure 8 shows the results of using ZPC with 0.3% bandwidth. Uneven illumination is apparent, but the effects can to a large extent be attributed to problems with the flat field image. Due to hardware difficulties, the flat field image was not a proper flat field, but rather a best fit of a displaced flat field. The symmetry of the fringing around each hole suggests that the beam was well centered in the hole of the lens. No special alignment steps were necessary. The longitudinal alignment was done by simply placing the center of the objective CRL in the back focal plane of the condenser, which was estimated theoretically from (2). The fact that the symmetry of the fringes is homogenous over the FOV suggests that a theoretical estimation was sufficient for longitudinal alignment in this case. The longitudinal spread of the focal spot was approximately $\Delta g_{ch}=\pm 8.8$ mm. The intensity in the focal spot could potentially reach a level where melting of the phase elements becomes an issue. In this case, the Zernike lenslet is a good choice of phase element as it passes the most intense part of the beam through less, rather than more material. It is difficult to judge from Figure 8 alone if deviation from the ideal phase shift is a problem, however, the phase shift imparted by the phase plate in the monochromatic experiment was estimated to be $0.18\pi+3\pi/2$. This deviation yielded ZPC, and is a much larger deviation than the inherent deviation associated with pink beam illumination. Δg_{ch} was estimated to 4.6 mm. The calculation takes into account the contribution to Δg_{ch} from the collector lenses. Assuming the central energy to be perfectly focused on the phase element, (22) result in $\sigma_{bg}=1.6$ µm, which is still not critically different from the idealized monochromatic value of $\sigma_{bg}=1.3$ µm. Had the monochromatic experiment been performed with $\Delta E/E=10^{-2}$, it would result in $\Delta g_{ch}=\pm 13.3$ mm. This gives $\sigma_{bg}=5.6$ µm, compared to $\sigma_{bg}=5.1$ µm in the monochromatic case. It is possible to reduce Δg_{ch} somewhat by using a condenser with a shorter focal length, but source size still dominates the ZPC performance with this modest band width. Note that (17) is somewhat strict when it comes to longitudinal misalignment. It is still possible to have ZPC even if the criterion above is not satisfied. If the spot is sufficiently small and well aligned transversally, but with a substantial longitudinal misalignment, a projection image of the phase plate could appear in the image plane. Inside the projection image there may still be ZPC, but such considerations will not be taken any further here as they would demand lengthy discussions about the defocus and coherence related blurring of the projection image.

The illumination scheme used in these experiments is useful for avoiding lateral chromatic aberration or artefacts from spatial filtering and field curvature. It also allows for insertion of the phase element into the objective. With visible light a more common technique is to employ Köhler illumination passed through an annular diaphragm, often referred to as hollow cone illumination. With FZPs for soft x-rays it is possible to produce what is sometimes referred to as pseudo Köhler illumination by employing a segmented zone plate [4]. The shape of the phase element may be a ring, concentric rings [17], or an array of spots [20]. The off-axis illumination associated with the use of a phase ring is expected to improve the resolution. Unfortunately, with absorbing CRLs, there is an unavoidable flux loss associated with increasing the angle of the hollow cone. A balance must be struck between flux and resolution. If the hollow cone is implemented by making use of an annular diaphragm, this represents adittional losses. However, with the advances made in manufacturing techniques of refractive optics, development of specialized condensers that plays the same role as segmented zone plates may be possible. Perhaps by some adaptation of rolled prism lenses [21], or by thickness modulation of standard lenslets could serve as a refractive equivalent of sectored zone plates. Condensers could conceivably be tailored to provide hollow cone illumination. It would still be possible to place the Fourier plane inside the objective by combining with standard CRLs, so that the phase element still may be fixed to the objective. Condensers like these could conceivably be used with FZPs too. It should however be noted that the main application area for CRL based microscopes, will be in studies of in situ processes, where both spatial and temporal resolutions must be considered.

5. Conclusion

It was demonstrated that ZPC can be implemented with x-ray CRLs with only small modifications to the standard microscopy setup.ZPC using x-ray CRLs was investigated and successfully implemented at 17 keV using Be-CRLs. While the traditional hollow cone illumination scheme is more appropriate when the goal is to optimize spatial resolution, there is still room for improvement of the resolution within the scheme described here, for example by reducing the size of the phase plate, using a shorter focal length objective, and increasing the magnification. It was also demonstrated that ZPC is achievable with illumination bandwidth of $\Delta E/E=0.3\times10^{-2}$, and arguments were presented that much larger bandwidths would be tolerable, which suggests that ZPC with pink beam illumination is feasible.

6. ACKNOWLEDGMENT

The authors would like to acknowledge the Norwegian Research Council (project grant no. 218404/F50), the Ministry of Education and Science of the Russian Federation (contract Nos. 14.Y26.31.0002) and the European Synchrotron Radiation Facility for supporting this work.

References

1. Zernike, F., *Phase contrast, a new method for the microscopic observation of transparent objects.* Physica, 1942. **9**(7): p. 686-698.
2. Schmahl, G., et al., *Phase contrast X-ray microscopy studies.* Optik, 1994. **97**(4): p. 181-182.
3. Neuhausler, U., et al., *X-ray microscopy in Zernike phase contrast mode at 4 keV photon energy with 60 nm resolution.* Journal of Physics D-Applied Physics, 2003. **36**(10a): p. A79-A82.
4. Takeuchi, A., K. Uesugi, and Y. Suzuki, *Zernike phase-contrast x-ray microscope with pseudo-Kohler illumination generated by*

sectored (polygon) condenser plate. 9th International Conference on X-Ray Microscopy, 2009. **186**.
5. Chen, J., et al., *Fresnel zone-plate based X-ray microscopy in Zernike phase contrast with sub-50 nm resolution at NSRL.* 9th International Conference on X-Ray Microscopy, 2009. **186**.
6. Holzner, C., et al., *Zernike phase contrast in scanning microscopy with X-rays.* Nature Physics, 2010. **6**(11): p. 883-887.
7. Chen, H., et al., *Quantitative phase retrieval in X-ray Zernike phase contrast microscopy.* Journal of Synchrotron Radiation, 2015. **22**: p. 1056-1061.
8. Shastri, S.D., P. Kenesei, and R.M. Suter, *Refractive lens based full-field x-ray imaging at 45-50 keV with sub-micron resolution.* X-Ray Nanoimaging: Instruments and Methods Ii, 2015. **9592**.
9. Kohmura, Y., et al., *Zernike phase-contrast X-ray microscope with an X-ray refractive lens.* Journal De Physique Iv, 2003. **104**: p. 603-606.
10. Simons, H., et al., *Full-field hard x-ray microscopy with interdigitated silicon lenses.* Optics Communications, 2016. **359**: p. 460-464.
11. Falch, K.V., et al., *Correcting lateral chromatic aberrations in non-monochromatic X-ray microscopy.* Applied Physics Letters, 2016. **109**(5): p. 054103.
12. Schroer, C.G., et al., *Magnified hard x-ray microtomography: Toward tomography with sub-micron resolution.* Developments in X-Ray Tomography Iii, 2002. **4503**: p. 23-33.
13. Simons, H., et al., *Extended formalism for simulating compound refractive lens-based x-ray microscopes.* ArXiv e-prints, 2016.
14. Edgcombe, C.J., *Imaging by Zernike phase plates in the TEM.* Ultramicroscopy, 2016. **167**: p. 57-63.
15. Kohn, V.G. and M.A. Orlov, *Theoretical analysis of the possibilities of Zernike phase contrast method in hard X rays for nondestructive imaging of micropipes in a silicon carbide single crystal.* Crystallography Reports, 2011. **56**(6): p. 941-946.
16. Dahle, A.K., et al., *Eutectic nucleation and growth in hypoeutectic Al-SI alloys at different strontium levels.* Metallurgical and Materials Transactions a-Physical Metallurgy and Materials Science, 2001. **32**(4): p. 949-960.
17. Vartiainen, I., et al., *Halo suppression in full-field x-ray Zernike phase contrast microscopy.* Optics Letters, 2014. **39**(6): p. 1601-1604.
18. Otaki, T., *Halo reduction technique in phase contrast microscopy.* Optical Review, 2001. **8**(4): p. 284-286.
19. Cheng, G.X., et al., *Zernike apodized photon sieves for high-resolution phase-contrast x-ray microscopy.* Optics Letters, 2010. **35**(21): p. 3610-3612.
20. Stampanoni, M., et al., *Hard X-ray Phase-Contrast Tomographic Nanoimaging.* 10th International Conference on X-Ray Microscopy, 2011. **1365**: p. 239-242.
21. Vogt, H., et al., *X-Ray Refractive Large Aperture Rolled Prism Lenses as Condensers for X-Ray Tubes.* Optical Design and Engineering Iv, 2011. **8167**.